JOURNAL OF APPLIED ELECTROCHEMISTRY 18 (1988) 909–914

A rechargeable redox battery utilizing ruthenium complexes with non-aqueous organic electrolyte

Y. MATSUDA, K. TANAKA, M. OKADA, Y. TAKASU, M. MORITA

Department of Industrial Chemistry, Faculty of Engineering, Yamaguchi University, Tokiwa-dai, Ube 755, Japan

T. MATSUMURA-INOUE

Department of Chemistry, Nara University of Education, Takabatake-cho, Nara 630, Japan

Received 8 February; revised 10 April 1988

A new-type redox battery has been developed. Some ruthenium complexes in organic electrolyte solution were utilized as the electrode active materials. A single cell consisting of $[Ru(bpy)_3]^{2+}$ complex in acetonitrile solution had an open circuit voltage of 2.6 V and a discharge current of 5 mA cm^{-2} (at a smooth carbon electrode). The characteristics of this type of cell were much influenced by such factors as the diaphragm material and the concentration of the complex. A cell with flowing electrolyte was also constructed and its charge–discharge performance was examined.

1. Introduction

Redox flow batteries are possible candidates for load-levelling devices in future energy systems. Up to the present, systems consisting of an iron–chromium couple in acidic media have been studied and developed as the most probable system [1]. However, problems such as the diaphragm of the cell must be overcome to realize a practical battery. Recently, we have proposed a new battery system which consists of a redox couple of transition-metal complex ions in a non-aqueous medium [2]. The principle of the cell is indicated in Equation 1,

$$\text{Positive electrode: } [ML_n]^{z+} = [ML_n]^{(z+1)+} + e^- \quad (1a)$$

$$\text{Negative electrode: } [ML_n]^{(z-1)+} = [ML_n]^{z+} + e^- \quad (1b)$$

where M is a transition metal such as ruthenium, iron, or osmium, L is a ligand (for example, 2,2′-bipyridine, ethylenediamine, 1,10-phenanthoroline), and n is the number of the ligand.

The special features of this system are a higher output voltage due to the use of a non-aqueous organic medium and a simpler cell system arising from the use of active materials of the same kind at both electrodes. The basic concept of this type of non-aqueous redox battery was first presented by Singh [3], but no experimental study has so far been carried out except our previous work [2], in which the principle of the cell operation and the fundamental discharge characteristics have been briefly demonstrated.

In the present work, we have examined some ruthenium or iron complexes such as $[ML_n]^{z+}$ in Equation 1, and acetonitrile as a non-aqueous solvent of the electrolyte. The properties of the electrolyte solution containing the active species, the charge–discharge characteristics of the cell and their dependences on the operating conditions were investigated. Points at issue concerning the practical use of batteries of this type are also discussed.

2. Experimental details

The metal complex mainly used here was tris(2,2′-bipyridine)ruthenium(II) tetrafluoroborate, $[Ru(bpy)_3](BF_4)_2$, which was prepared and purified by the method described in the literature [4]. The solvent, acetonitrile (CH_3CN), was reagent grade, and was dehydrated and purified by a routine distillation method [5] before use. In most experiments tetraethylammonium tetrafluoroborate (Et_4NBF_4) was used as a supporting electrolyte.

An H-type glass cell was mainly used for the electrochemical measurements. Figure 1 shows a sketch of the cell, where the diaphragm is exchangeable. It was used for the measurements of the half-cell characteristics. The test electrode was a smooth glassy carbon (GC) plate (6.5 cm^2). The counter and reference electrodes were a GC plate (13.0 cm^2) and an Ag/Ag^+ electrode, respectively. Before the electrochemical measurements, the GC plate was polished with fine alumina powder followed by washing with redistilled water and acetone in an ultrasonic cleaner. The diaphragms used in the experiments were (1) sintered glass (a glass filter #4), (2) an anion exchange membrane (AEM) (Neocepta ACH-45T, Tokuyama Soda), (3) a porous polymer-hybrid membrane (MF-2508 or YS-UE02-4B, Yuasa Battery), and (4) a porous fluorocarbon resin filter (Polyflon PF-1 or PF-3, Toyo Roshi). The volume of the electrolyte was

0021-891X/88 $03.00 + .12

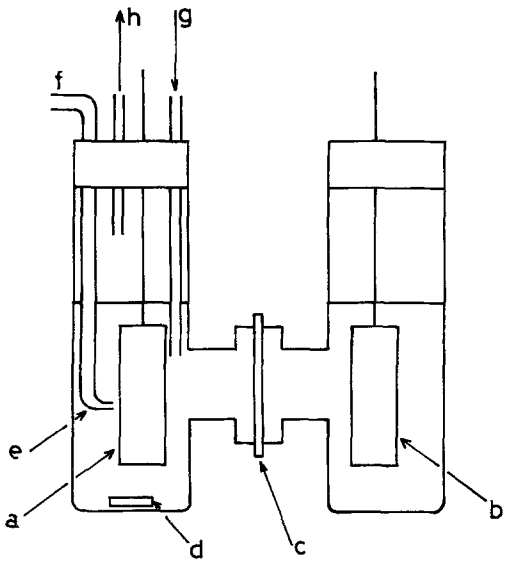

Fig. 1. An H-type cell for electrochemical measurements, (a) test electrode (GC plate), (b) counter electrode (GC plate), (c) diaphragm, (d) stirrer piece, (e) Luggin capillary, (f) to the reference electrode, (g) nitrogen gas inlet, (h) nitrogen gas outlet.

13 cm^3 in each compartment. A similar H-type cell (inner volume = 50 cm^3) with a glass filter diaphragm was used for the full-cell experiments. In this case the electrodes were felts of carbon fibre (GF-25A, Nihon Carbon; apparent area 10 cm^2) with graphite-rod current-collectors. This form of the cell will be mentioned as 'the static H-cell" distinguished from 'the flow-type cell', though the electrolytes in the former cell were slowly stirred magnetically throughout the experiment. The real surface area of the electrode is much larger than the apparent area, especially in the case of the felt electrode. However, all the current densities in this paper will be based on the geometric surface area of the electrode, i.e. they are apparent current densities.

In most cases the cell was charged potentiostatically (for half-cell tests) or under a constant voltage (for full-cell tests). The charging electricity was preset so that a half of the active material (the Ru(II) complex) would be theoretically converted to Ru(III) (at the positive electrode) and Ru(I) (at the negative electrode). That is, the depth of charge was 50%. In some cases, steady-state polarization curves were potentiostatically measured. The discharge was carried out under constant-current conditions until the potential or the cell voltage reached preset values. The charge–discharge cycle was generally repeated at least five times. The polarization curves were measured after 50% charge. These experiments were carried out under a dry nitrogen atmosphere in a light-shielded bath at 25° C.

Figure 2 shows a schematic diagram for the experimental system with a flow-type cell. The dimensions of the cell were 160 × 55 × 30 mm^3. Carbon fibre cloth (Toyobo; 120 × 10 × 1 mm^3) was used as the electrode (current-collector). The thickness of the Teflon spacer was 1.0 mm. The diaphragm was AEM. The electrolyte circulated in a parallel flow from the bottom to the top of the cell. The electrolyte reservoirs

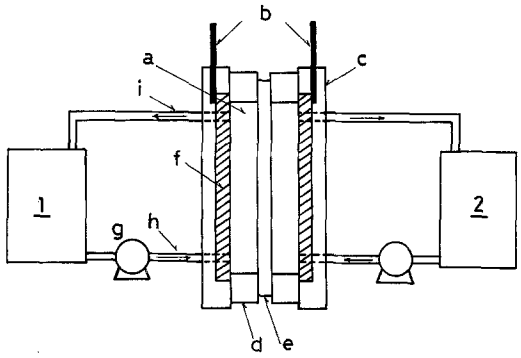

Fig. 2. Schematic diagram of the flow-type cell system, (a) carbon fibre cloth, (b) terminal leads, (c) cell case, (d) Teflon spacer, (e) diaphragm (AEM), (f) current-collector, (g) pump, (h) electrolyte inlet, (i) electrolyte outlet, *1* anolyte tank, *2* catholyte tank.

were shielded from the light and blanketed with dry nitrogen. The cell was charged under a constant voltage and discharged under a constant current at room temperature (20–28° C).

3. Results and discussion

The voltammetric behaviour of $[Ru(bpy)_3]^{2+}$ in organic media has been studied by many workers [6–9]. Figure 3 shows a typical cyclic voltammogram obtained in this work for $[Ru(bpy)_3](BF_4)_2$ at a smooth GC electrode (0.096 cm^2) in CH_3CN containing Et_4NBF_4 (0.1 mol dm^{-3}) as the supporting electrolyte. Four redox couples are observed in this potential region. The couple at the highest anodic potential (~ 1.0 V vs Ag/Ag^+), a_1/c_1, is based on the redox reaction $[Ru(bpy)_3]^{2+}/[Ru(bpy)_3]^{3+}$ (i.e. Ru(II)/Ru(III), Equation 2). The others, a_2/c_2, a_3/c_3 and a_4/c_4 are attributed to Equations 3, 4 and 5, respectively.

$$[Ru(bpy)_3]^{2+} = [Ru(bpy)_3]^{3+} + e^- \quad (2)$$

$$[Ru(bpy)_3]^{+} = [Ru(bpy)_3]^{2+} + e^- \quad (3)$$

$$[Ru(bpy)_3]^{0} = [Ru(bpy)_3]^{+} + e^- \quad (4)$$

$$[Ru(bpy)_3]^{-} = [Ru(bpy)_3]^{0} + e^- \quad (5)$$

The peak separation ($\Delta E = E_a - E_c$) shows that each reaction proceeds almost reversibly [6, 9]. Figure

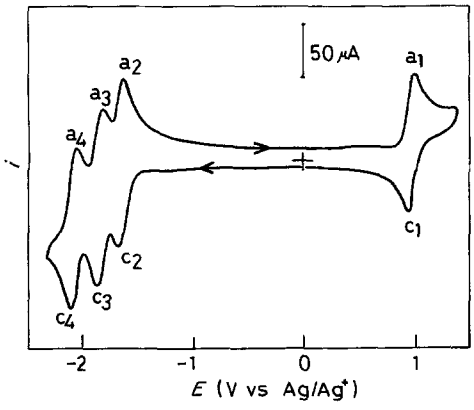

Fig. 3. Cyclic voltammogram of $[Ru(bpy)_3](BF_4)_2$ at GC electrode in Et_4NBF_4 (0.1 mol dm^{-3})/CH_3CN. Concentration of $[Ru(bpy)_3](BF_4)_2$ = 2 × 10^{-3} mol dm^{-3}, electrode area = 0.096 cm^2, potential scan rate = 0.3 V s^{-1}, temperature = 30° C.

Table 1. Conductivity of the electrolytic solution at 30° C

Complex (Conc., mol dm^{-3})	*Conc. of supporting electrolyte* (mol dm^{-3})*	*Conductivity (10^{-2} S cm^{-1})*
	0	1.20
$[Ru(bpy)_3](BF_4)_2$	0.5	4.66
(0.15)	1.0	6.11
	1.5	6.90
$[Ru(bpy)_3](BF_4)_2$	0	1.04
(0.05)	0.5	4.39
$[Fe(bpy)_3](BF_4)_2$	0	1.01
(0.05)	0.5	4.74
$[Ru(bpy)_3](ClO_4)_2$	0	1.12
(0.05)	0.5**	4.62

* $(C_2H_5)_4NBF_4$, ** $(C_2H_5)_4NClO_4$.

3 also shows that the combination of Reactions 2 and 3 leads to a redox battery with an open-circuit voltage (OCV) of about 2.6 V [2]. Similar voltammograms were obtained for $[Fe(bpy)_3]^{2+}$ and $[Ru(acac)_3]$ (acac is acetylacetonato) in CH_3CN solution. Those voltammograms suggested that the combinations of $[Fe(bpy)_3]^{2+}/[Fe(bpy)_3]^{3+}$ and $[Fe(bpy)_3]^{+}/[Fe(bpy)_3]^{0}$, and $[Ru(acac)_3]/[Ru(acac)_3]^{+}$ and $[Ru(acac)_3]^{-}/[Ru(acac)_3]$ would form batteries with an OCV of about 2.5 V and 1.6 V, respectively. In this paper, however, we have mainly examined the cell utilizing the $[Ru(bpy)_3]^{2+}$ system, because its basic characteristics such as chemical stability in organic media are relatively superior to those of the others.

The conductivity of the electrolyte solution is of special importance in practical batteries as it is directly related to the internal resistance of the cell. The conductivity of ruthenium salt solutions measured at 30° C by an a.c. bridge method is listed in Table 1. In the solutions without supporting electrolytes, the conductivity was 1.0–1.2 × 10^{-2} S cm^{-1}. The concentration dependence of the conductivity was rather small in the concentration range 0.05–0.15 mol dm^{-3}. The solubilities of the salts in CH_3CN were about 0.2 mol dm^{-3} for $[Ru(bpy)_3](BF_4)_2$ and 0.8 mol dm^{-3} for $[Fe(bpy)_3](BF_4)_2$. Addition of the tetraethylammonium salt was effective for conductance enhancement. The conductivity of 4–7 × 10^{-2} S cm^{-1} for the solutions containing the supporting electrolyte will be usable for practical batteries.

Figure 4 shows steady-state polarization curves for the redox reactions of $[Ru(bpy)_3](BF_4)_2$ measured at a smooth GC electrode after 50% charge of the cell with the sintered glass diaphragm. The potentiostatic charging was carried out at 1.1 V and −1.9 V vs Ag/Ag^+ for the positive and the negative electrodes, respectively. The anodic and cathodic currents at the positive and the negative electrodes correspond to the respective reactions described in the figure. At the positive electrode, the anodic and cathodic curves are almost symmetrical, suggesting that the reactions proceed reversibly. The limiting current density was 3–4 mA cm^{-2} under these experimental conditions. On the other hand, the polarization curves at the negative

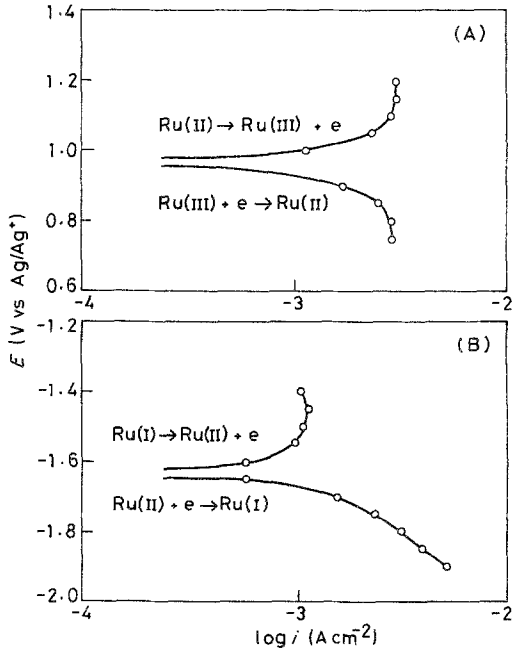

Fig. 4. Steady-state polarization curves at GC electrode after 50% charge of the H-type cell. Electrolyte is Et_4NBF_4 (0.1 mol dm^{-3})/CH_3CN containing 2 × 10^{-2} mol dm^{-3} of $[Ru(bpy)_3](BF_4)_2$. (A) Positive electrode (charged at 1.1 V), (B) Negative electrode (charged at −1.9 V).

electrode were quite asymmetrical. No limiting current was observed during the cathodic polarization. The anodic current was saturated at about 1 mA cm^{-2}, which is much lower than the limiting current at the positive electrode. This suggests that the cathodic charging process (Ru(II) + e^- → Ru(I)) was accompanied by side reactions and that the process was insufficient for yielding the theoretical amount of Ru(I).

The galvanostatic discharge curves at the positive electrode are shown in Fig. 5. The utilization on the abscissa indicates the percentage of the coulombs with respect to the amount of electricity passed in the charge. The discharge profile changed slightly on repeating the charge–discharge cycle. The curves shown in the figure are for the second discharge. The coulombic efficiency (the utilization where the elec-

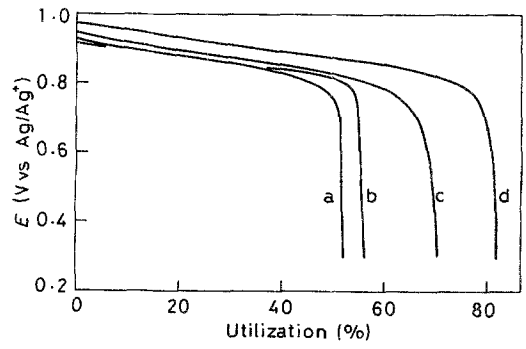

Fig. 5. Galvanostatic discharge curves of the positive electrode in the H-type cell with various diaphragms after 50% charge at constant potential (1.1 V). Electrolyte is Et_4NBF_4 (0.1 mol dm^{-3})/CH_3CN containing 2 × 10^{-2} mol dm^{-3} of $[Ru(bpy)_3](BF_4)_2$, discharge current = 1 mA (electrode area = 6.5 cm^2), diaphragms are (a) sintered glass filter, (b) polymer-hybrid membrane (YS-UE02-4B), (c) AEM (ACH-45T), (d) Polyflon filter (PF-3).

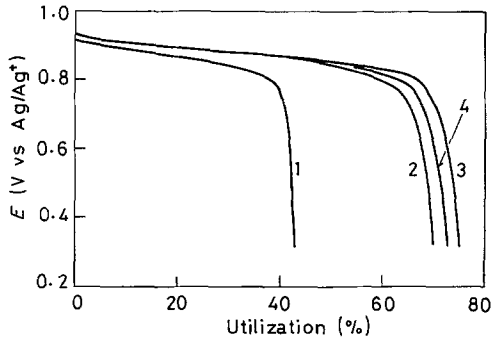

Fig. 6. Galvanostatic discharge curves of the positive electrode in the H-type cell with the AEM diaphragm after 50% charge at constant potential (1.1 V). Electrolyte is Et_4NBF_4 (0.1 mol dm^{-3})/CH_3CN containing 2×10^{-2} mol dm^{-3} of $[Ru(bpy)_3](BF_4)_2$, discharge current = 1 mA (electrode area = 6.5 cm^2), figures on the curves indicate the cycle number.

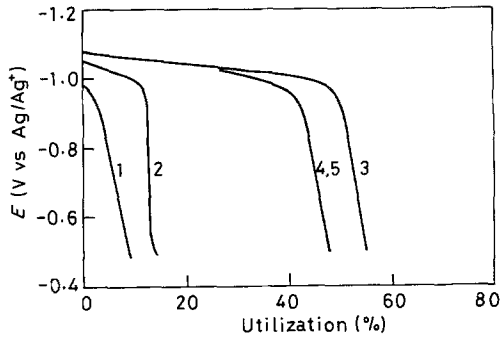

Fig. 8. Galvanostatic discharge curves of the negative electrode in the H-type cell with the AEM diaphragm after 50% charge at constant potential (−1.2 V). Electrolyte is Et_4NBF_4 (0.1 mol dm^{-3})/CH_3CN containing 2×10^{-2} mol dm^{-3} of $[Ru(acac)_3]$, discharge current = 1 mA (electrode area = 6.5 cm^2), figures on the curves indicate the cycle number.

trode potential falls to about 0 V vs Ag/Ag^+) was 50–80%, and was dependent on the diaphragm of the cell. The Polyflon filter diaphragm gave the highest efficiency at the positive electrode, but had the highest voltage drop. Lower efficiencies were observed in the cells with diaphragms of relatively large pore size; the sintered glass filter and the polymer-hybrid membrane. This means that the migration of the electroactive species (ruthenium complexes) between the anodic and cathodic compartments would be one of the major reasons for the efficiency loss during the charge–discharge cycle in this type of the cell.

Typical variation of the discharge profile at the positive electrode in the cell with an AEM diaphragm is shown in Fig. 6. The AEM diaphragm was the best with respect to the ion transport and the electrolyte separation. However, the coulombic efficiency was at most 70%. This result suggests that the current flow in the diaphragm did not proceed only through the ion exchange mechanism. The migration of the active species would occur from the one compartment to the other through micropores in the membrane as an additional mechanism. The low efficiency in the first cycle is probably related to a small amount of water in the membrane.

The discharge curves at the negative electrode are shown in Fig. 7, where the AEM was used as the diaphragm. The coulombic efficiency was much lower than that of the positive electrode and varied with the charge–discharge cycle. Similar results were obtained in the cells with the other diaphragms. As mentioned in the results of the polarization curves in Fig. 4, these low efficiencies of the negative electrode are probably caused by insufficient charging (i.e. some side reaction during the charge) and/or the chemical instability of the reduced species, Ru(I). The former may involve the cathodic reduction of the Et_4N^+ ion of the supporting electrolyte and the latter is possibly due to degradation of the ruthenium complex. However, the irreversibility of the Ru(I)/Ru(II) system has scarcely come into question in previous voltammetric studies.

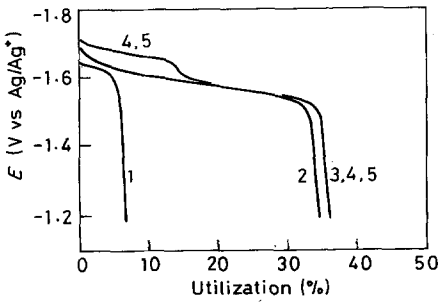

Fig. 7. Galvanostatic discharge curves of the negative electrode in the H-type cell with the AEM diaphragm after 50% charge at constant potential (−1.9 V). Electrolyte is Et_4NBF_4 (0.1 mol dm^{-3})/CH_3CN containing 2×10^{-2} mol dm^{-3} of $[Ru(bpy)_3](BF_4)_2$, discharge current = 5 mA (electrode area = 6.5 cm^2), figures on the curves indicate the cycle number.

The discharge performance of the negative electrode can be improved by substituting the organic ligand of the complex. Figure 8 shows the discharge curves of the negative electrode using an $[Ru(acac)_3]$ system. As $[Ru(acac)_3]^-$ is chemically stable compared with $[Ru(bpy)_3]^+$, a relatively high efficiency was obtained, except for the early cycles.

Figure 9 shows the efficiencies of the positive and negative electrodes as a function of the discharging current. The potentiostatic charging conditions were constant throughout the experiment (+1.1 V and −1.9 V vs Ag/Ag^+ for the positive and negative electrodes, respectively). The efficiency of the positive electrode was as high as about 60% up to a current of

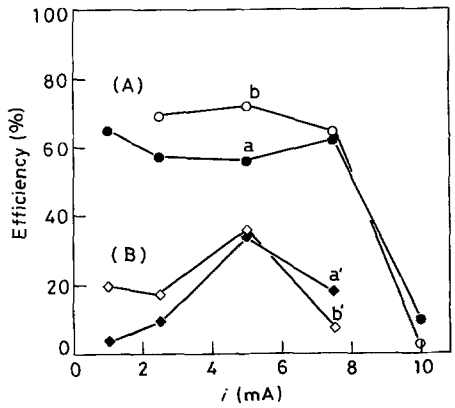

Fig. 9. Discharge efficiencies of the positive (A) and negative (B) electrodes as a function of the discharge current. Electrolyte is Et_4NBF_4 (0.1 mol dm^{-3})/CH_3CN containing 2×10^{-2} mol dm^{-3} of $[Ru(bpy)_3](BF_4)_2$, the electrode area = 6.5 cm^2, a and a′ are at the second discharge, b and b′ are at the fifth discharge.

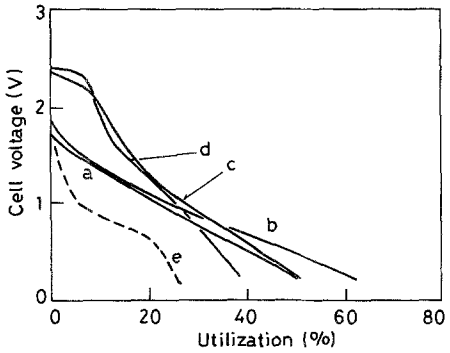

Fig. 10. Discharge curves of the H-type cell with the sintered glass filter diaphragm after 50% charge at constant voltages. Electrolyte is Et_4NBF_4 (0.1 mol dm^{-3})/CH_3CN containing $[Ru(bpy)_3](BF_4)_2$ (a–d), or Et_4NClO_4 (0.5 mol dm^{-3})/CH_3CN containing 2×10^{-2} mol dm^{-3} of $[Fe(bpy)_3](BF_4)_2$ (e), (a) [Ru complex] = 2×10^{-2} mol dm^{-3}, 3.0 V charge, 1 mA discharge, (b) [Ru complex] = 2×10^{-2} mol dm^{-3}, 3.1 V charge, 1 mA discharge, (c) [Ru complex] = 5×10^{-2} mol dm^{-3}, 3.0 V charge, 2 mA discharge, (d) [Ru complex] = 1.5×10^{-1} mol dm^{-3}, 2.9 V charge, 2 mA discharge, (e) [Fe complex] = 2×10^{-2} mol dm^{-3}, 3.0 V charge, 1 mA discharge.

7.5 mA (1.15 mA cm^{-2}), but it decreased significantly at the 10 mA discharge rate. It is considered that the higher discharge current results in high concentration polarization which can cause some undesirable side reactions. On the other hand, a maximum efficiency (about 35%) was observed at 5 mA (0.77 mA cm^{-2}) for the discharge of the negative electrode. The lower efficiencies at lower current densities are probably related to the longer discharging times needed. That is, the loss of the active Ru(I) complex would increase with decrease in the discharge current.

The efficiencies at the positive and negative electrodes depended on the concentration of the active complex. The concentrations of 0.02–0.05 mol dm^{-3} gave maximum efficiencies at the positive electrode. The efficiency tended to be rather lower in the cells with higher concentration (> 0.1 mol dm^{-3}) of the ruthenium complex. This is probably due to the fact that in such cells the migration of the electrolyte through the diaphragm proceeds readily. The lower concentration (< 0.01 mol dm^{-3}) of the complex gave very low efficiencies. A similar tendency was observed for the concentration dependence of the efficiency at the negative electrode.

The discharge curves of the full cell with the sintered glass filter diaphragm are shown in Fig. 10, where various charge–discharge conditions were examined. The charging was carried out under constant voltage and the depth of charge was 50%. In these cells, the electrolytic solutions did not circulate. The shape of the discharge curve depended on the current density. The operating cell voltage was somewhat lower than the potential difference between each electrode because of the potential drops within the electrolyte and the diaphragm. The efficiency of the cell with the ruthenium complex was 35–40% if one defines the cut-off voltage of the cell to be about 0.5 V. It is considered that the performance of the full cell is limited by that of the negative electrode. The cell

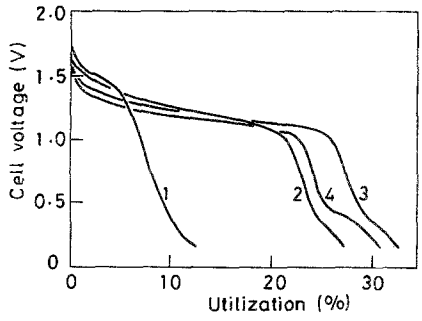

Fig. 11. Discharge curves of the flow-type cell with the AEM after 50% charge at constant voltage (3.0 V). Electrolyte is Et_4NBF_4 (0.1 mol dm^{-3})/CH_3CN containing 2×10^{-2} mol dm^{-3} $[Ru(bpy)_3](BF_4)_2$, flow rate = 0.18 cm^3 s^{-1}, pre-immersion time of the AEM in CH_3CN = 3 h.

utilizing the iron complex showed a relatively low efficiency.

Figure 11 shows the discharge profile of the flow-type cell with the $[Ru(bpy)_3](BF_4)_2$ system and the AEM diaphragm. Charging was carried out with a constant cell voltage of 3.0 V, and the flow rate of the electrolyte was 0.18 cm^3 s^{-1}. The variation of the cell voltage during the discharge was less than that of the cell with static electrolytes (c.f. Fig. 10). As the inter-electrode distance in the flow-type cell was much smaller than that in the static H-cell, the ohmic loss in the electrolyte of the flow-type cell would be lower than that of the static H-cell. The low efficiency at the first discharge is probably influenced by a small amount of water in the AEM diaphragm although the membrane had been immersed in CH_3CN for 3 h before use. On the other hand, swelling of the AEM during contact with the organic electrolyte led to decreasing efficiency with further cycling. As shown in Fig. 12, shortening of the pre-immersion time of the AEM in CH_3CN resulted in an improvement of the efficiency, except for the first two cycles. By comparing the results shown in Figs 10–12, the flatness of the discharge curve and the coulombic efficiency tended to be improved by flowing the electrolyte, which prevents the active species reduced at the negative electrode from degradation. It seems that there is an optimum rate of the electrolyte flow (for example, about 0.18 cm^3 s^{-1} for the complex concentration of

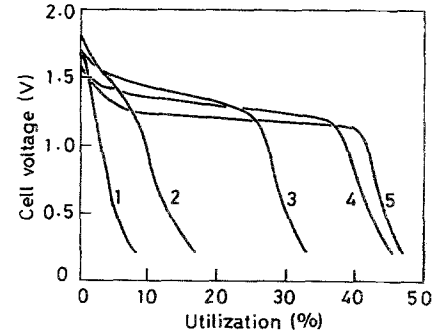

Fig. 12. Discharge curves of the flow-type cell with the AEM after 50% charge at constant voltage (3.0 V). Electrolyte is Et_4NBF_4 (0.1 mol dm^{-3})/CH_3CN containing 2×10^{-2} mol dm^{-3} $[Ru(bpy)_3](BF_4)_2$, flow rate = 0.18 cm^3 s^{-1}, pre-immersion time of the AEM in CH_3CN = 20 min.

$0.02\,mol\,dm^{-3}$ in this cell). Such technical investigations as the cell structure, the flow system and the operating conditions, as well as the search for more effective metal complexes, will be necessary to make practical redox batteries of commercial reality.

4. Conclusion

A new redox battery with metal complexes in an organic electrolyte solution has been proposed, and its basic behaviour investigated. The results are summarized as follows.

(1) About 2.6 V of OCV and $5\,mA\,cm^{-2}$ of discharge current were obtained for the system $[Ru(bpy)_3](BF_4)_2/CH_3CN$.

(2) The reversibility of the negative electrode largely controlled the charge–discharge performance of the full cell. The charge–discharge efficiency at the positive electrode was about 70%, while the efficiency at the negative electrode was 20–40% under the same conditions.

(3) The characteristics of the diaphragm influenced the cell performance considerably. Relatively high efficiencies were obtained when diaphragms with a small pore size or selective permeability were used.

(4) The efficiency at the negative electrode was somewhat improved by using flowing electrolyte. A flow-type cell with an AEM diaphragm showed an efficiency of about 40%.

Acknowledgements

This work was financially supported by Grants-in-Aid for Scientific Research Nos 59040053, 60040055, and 61040019 from the Japan Ministry of Education, Science and Culture. We also wish to thank Mr Yoshinori Tanaka for his assistance in the voltammetric experiments. Also, we are grateful to Mr M. Yoshitake and Mr O. Hamamoto of the Mitsui Engineering and Shipbuilding Co. Ltd. for their helpful discussion and for supplying the flow cell and materials.

References

[1] N. H. Hagedorn, 'NASA Redox Storage System Development Project – Final Report', DOE/NASA/12726-24, NASA TM-83677, US Department of Energy, October 1984.
[2] Y. Matsuda, Y. Takasu, M. Morita, K. Tanaka, M. Okada and T. Matsumura-Inoue, *Denki Kagaku* **53** (1985) 632.
[3] P. Singh, *J. Power Sources* **11** (1984) 135.
[4] C. F. Liu, N. C. Liu and J. C. Bailar, Jr, *Inorg. Chem.* **3** (1964) 1085.
[5] C. K. Mann, 'Electroanalytical Chemistry' Vol. 3 (edited by A. J. Bard), Marcel Dekker, New York (1969) p. 57.
[6] T. Saji and S. Aoyagui, *J. Electroanal. Chem.* **63** (1975) 31.
[7] C. R. Martin, I. Rubinstein and A. J. Bard, *ibid.* **151** (1983) 267.
[8] T. Matsumura-Inoue, C. Ishida, M. Kasai and N. Kuroda, *Nippon Kagaku Kaishi* **1982** (1982) 72.
[9] M. Morita, Y. Tanaka, K. Tanaka, Y. Matsuda and T. Matsumura-Inoue, *Bull. Chem. Soc. Jpn*, in press.